

# A NEW METHOD OF IMPULSE NOISE REDUCTION IN GRAY AND COLOR IMAGES BY FUZZY FILTER

M.Harikrishnan  
Department of Mathematics  
Kongu Engineering College  
Erode, India

R.Viswanathan  
Department of Mathematics  
Kongu Engineering College  
Erode, India

**Abstract:** Image Reduction is one of the most important image processing tasks. In this article, a new fuzzy filter is presented for the removal of impulse noise in gray and color images. The filter consists of two stages. In the first stage, using trapezoid membership function four values are used to detect whether a given pixel contains noise or not. In the second stage fuzzy enhanced classifier is applied successively to remove the impulse noise in gray and color images. Experimental results are obtained to show the feasibility of the proposed approach. These results are also compared to other filters by numerical measures and visual inspection.

**Keywords :** Threshold, impulse noise, denoising, fuzzy filter, fuzzification, defuzzification

## 1. INTRODUCTION

Image processing has become a very important subject in electronic and computer engineering. Image processing has got wide varieties of applications in computer vision, multimedia communication, and television broadcasting etc., that demand very good quality of images.

### 1.1 NOISE

An image gets corrupted with noise during the process of acquisition, transmission, storage and retrieval. Noise may be classified as substitutive noise, impulsive noise (salt and pepper noise, random valued impulse noise etc.) and additive noise e.g. additive with Gaussian noise. Image restoration is one of the many areas it encompasses.

#### 1.1.1 Impulse Noise

The probability density function of impulse noise is given by

$$P(z) = \begin{cases} P_a & \text{for } z = a \\ P_b & \text{for } z = b \\ 0 & \text{otherwise} \end{cases}$$

If  $b > a$ , gray level  $b$  will appear as a light dot in the image. Impulse noise is generally digitized as pure white or black values in an image. If they are equal to the minimum and maximum allowed values in the digitized image, they are called standard values. As a consequence, negative impulses appear as black (pepper) points in an image. Positive impulse appears as white (salt) noise. In a 8 bit image,  $a=0$ (black) and  $b=255$  (white). Fat fail distributed or impulse noise is sometimes called salt& pepper noise or spike noise. An image containing salt & pepper noise will have dark pixels in bright regions & bright pixels in dark regions. This type of noise can be caused by analog to digital convertor errors, bit errors in transmission etc.

### 1.2 IMAGE DENOISING

It is one of the main areas of image restoration. Image

denoising is usually required to be performed before display or further processing like segmentation feature extraction, object recognition, texture analysis etc. The purpose of denoising is to suppress the noise quite efficiently while retaining the edges and other detailed features as much as possible. It becomes necessary to suppress the noise quite effectively without distorting the edges and the fine details of the image so that the filtered image becomes more useful for display and/or further processing. The nature of denoising depends on the type of the noise corrupting the image. S. Schulte et.al [1] proposed a filter removing random impulse noise using fuzzy random method and Stefan Schulte et.al [2] presented a fuzzy filter to remove noises in color images.. Morillas,S et al [3] presented fuzzy bilateral filtering for color images.In the literature [4]-[9], there are many methods available to remove impulse noise in gray scale and color images. Many filtering techniques over decades serve better for the enhancement of the images.Of these, median Filter is the non- linear filter in which sorting operation is performed on the input vector. The job is done as the mid value is taken as the input. Moving average filter overcomes the drawback of the median filter by using moving average in which the value at the central pixel is replaced by the mean value of the corresponding input neighborhood. Entropy filter denoises image by replacing every value by the information entropy of the values in its range  $r$  neighborhood. The range filter allows to select a range of values. The left and right drag box can be used to change the lower and upper limit of the range, meaning that only rows with values within the chosen range remain in the visualization. An important feature of the range filter is that the values are distributed on a linear scale according to the values of the data. Standard filter filters image by replacing every value by the standard deviations of the values in its range  $r$  neighborhood. This paper deals with a new fuzzy filtering technique for the removal of impulsive noise in both gray and color images. Fuzzy filters are easy to realize by means of simple fuzzy rules.

## 2. PROPOSED NEW FUZZY FILTER FOR IMPULSE NOISE REDUCTION IN GRAY AND COLOR IMAGES

This paper focuses on developing a new filter to remove impulse noise in gray and color images. The proposed filter uses fuzzy trapezoid membership function to remove impulse noise in the image. Let  $f(x, y)$  and  $f'(x,y)$ denote the pixel value at location  $(x,y)$

of the given input image and the image with the noise respectively.  
 The impulse noise detection with noise  $\alpha$  is given as follows

$$f(x, y) = \begin{cases} f_{x,y} & \text{with the probability } \alpha \\ Q_{x,y} & \text{with probability of } 1-\alpha \end{cases} \quad (2.1)$$

where  $f_{x,y}$  denotes the noise value

$$\text{Deten}_i = \text{abs}(f'_x - f'_y) \quad (2.2)$$

By using fuzzy trapezoid membership classification, four values are used to detect whether a given pixel contains noise or not. The trapezoid membership classification is used because the deployment of the trapezoidal membership function is better than the triangular membership function. In addition, trapezoidal function provides the optimal degree of compatibility for higher levels of attributes than the triangular function. At the same time, it is provided with the maximum membership value which corresponds to the centroid of the triangular shape. As a result, the application of trapezoidal membership function using enhanced fuzzy classifier gives higher degrees of compatibility resulting in the approximation of the desired output. To use trapezoidal membership function, four parameters are necessary as given in figure 2.1, and so 4 x 4 matrix is used.

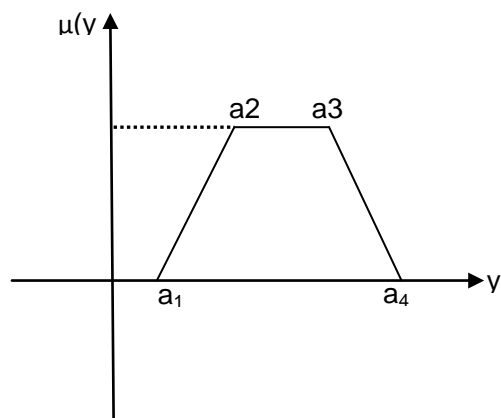


Figure 2.1 Trapezoidal membership function

By applying the trapezoidal membership function, initially,  $\text{Deten}_i$  is mapped onto range [0,100] and are classified into two partitions. The two partitions comprise low  $\text{Deten}_i$  (L) and high intensity  $\text{Deten}_i$  (H) respectively using two different thresholds, namely  $T_1$  and  $T_2$ .

```

If ( $\text{Deten}_i$  is in range (0,  $T_2$ ))
{pixel is classified as  $\text{Deten}_i$  (L)}
Else
If ( $\text{Deten}_i$  is in range ( $T_1$ , 100))
{pixel is classified as  $\text{Deten}_i$  (H)}
Endif
    
```

Let us consider a scenario, a process followed to restore the noisy images.

Table 2.1 Impulse noise reduction process

|     |     |     |     |     |     |     |     |
|-----|-----|-----|-----|-----|-----|-----|-----|
| 240 | 120 | 120 | 120 | 240 | 250 | 180 | 120 |
| 240 | 120 | 120 | 120 | 240 | 120 | 120 | 120 |
| 240 | 120 | 120 | 120 | 240 | 120 | 120 | 120 |
| 240 | 120 | 120 | 120 | 240 | 120 | 120 | 120 |

a) pixel-original image                      b) Pixel – noisy image

|     |     |     |     |
|-----|-----|-----|-----|
| 240 | 120 | 160 | 120 |
| 240 | 120 | 120 | 120 |
| 240 | 120 | 120 | 120 |
| 240 | 120 | 120 | 120 |

(c) noisy image removed

|     |     |     |     |
|-----|-----|-----|-----|
| 240 | 120 | 120 | 120 |
| 240 | 120 | 120 | 120 |
| 240 | 120 | 120 | 120 |
| 240 | 120 | 120 | 120 |

(d) noisy image completely removed

The motivation for Impulse noise detection and filtering using Fuzzy Classification of noisy images is illustrated as follows. In Table 2.1(a), the original image of a pixel is shown. Let us consider that the two pixels in the image block comprise of impulse noise with the respective noisy pixel values as 250 and 180 as illustrated in Table 2.1(b). Then, in this case scenario, let us assume that the locations of these two impulse noisy pixels are detected and replaced using enhanced fuzzy classification as shown in Table 2.1(c).

When compared with Table 2.1(a) and Table 2.1(c), one noisy pixel is restored after application of first membership function. The impulse noisy pixel value 180 is replaced with the value of 160 which also comprise of impulse noise pixel value when compared to the actual original pixel value of the corresponding image. Subsequently, if we repeat the same process by applying the membership function, then both noisy pixels are removed as illustrated in Table 2.1 (d).

The original cameraman image, the impulse noise image is shown in figure 2.2.

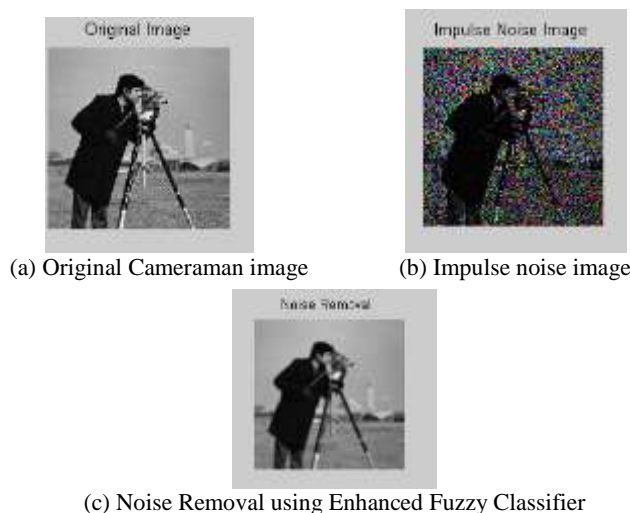


Figure 2.2 Impulse Noise Reduction Process

The quality of images using fuzzy classification is measured by means of peak signal-to-noise ratio (PSNR), detection accuracy and noise level.

### 3. Experimental Results Impulse noise detection and filtering using Enhanced Fuzzy Classifier

In order to assess the performance of the proposed Impulse Noise Removal using Enhanced Fuzzy Classifier (INREFC), extensive simulations are carried out on standard gray and color images of cameraman under different noisy conditions in MATLAB. The performance is measured in terms of Peak Signal-to-Noise Ratio (PSNR) detection accuracy and noise level.

PSNR is defined as

$$\text{PSNR} = 10 \log_{10} \left( \frac{255^2}{\text{MSE}} \right) \text{dB}$$

Detection accuracy is defined as

$$\text{Detection Accuracy} = \sqrt{\frac{1}{N} \sum_{i=1,2,\dots,N} (x_i^2 + y_i^2)}$$

### 3.1 Measure of PSNR

The table 1 given below shows the peak signal-to-noise rate for different image sizes which is obtained using gray images of cameraman.

**Table 3.1 Measure of PSNR**

| Image Size (pixels) | PSNR (dB)       |                |              |                 |
|---------------------|-----------------|----------------|--------------|-----------------|
|                     | Proposed INREFC | Entropy Filter | Range Filter | Standard Filter |
| 150                 | 93              | 90.25          | 89.5         | 86.25           |
| 200                 | 93.55           | 92.55          | 90.25        | 85              |
| 250                 | 95              | 94.5           | 93.35        | 88              |
| 300                 | 96.5            | 96             | 94.55        | 90              |

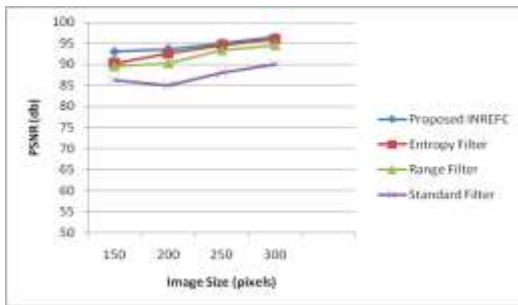


**Figure 3.1 Image Size Vs PSNR**

The figure 3 shows the measure of PSNR for both color and gray images for impulse noise detection and filter using enhanced fuzzy classifier. A detailed comparison analysis is made using three other filters, standard filter, range filter and entropy filter. From the figure, it is evident that the peak signal-to-noise ratio is comparatively higher using enhanced fuzzy classifier when compared to other three filters. The PSNR rate is high using enhanced fuzzy classifier due to the fact that trapezoid membership classification is used with a variance of 3-5% of signal-to-noise ratio increased when compared to entropy filter, 5% of signal-to-noise ratio increased when compared to range filter.

### 3.2 Measure of Detection Accuracy

The table 3.2 given below shows the detection accuracy rate for different image sizes which is obtained using color and gray images of cameraman.

**Table 3.2 Measure of Detection Accuracy**

| Image Size (pixels) | Detection Accuracy (%) |                |              |                 |
|---------------------|------------------------|----------------|--------------|-----------------|
|                     | Proposed INREFC        | Entropy Filter | Range Filter | Standard Filter |
| 150                 | 65                     | 58             | 55           | 53              |
| 200                 | 70                     | 60             | 58           | 55              |
| 250                 | 72                     | 65             | 60           | 52              |
| 300                 | 75                     | 68             | 62           | 54              |

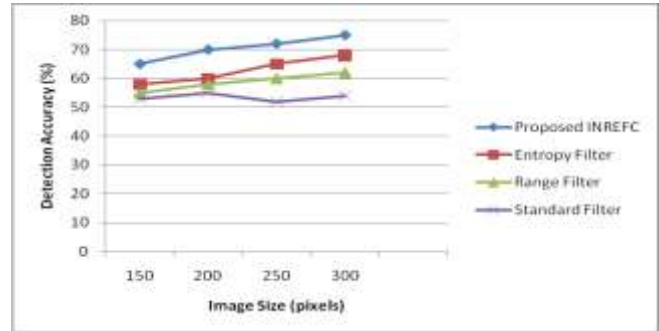


**Figure 3.2 Image Size Vs Accuracy**

Figure 3.2 describes the accuracy level of both color and gray image of cameraman using Enhanced Fuzzy Classifier. The detection accuracy level of the image is measured in terms of %. When the size of image which is measured in terms of pixels gets increased, the detection accuracy is reduced. But when compared with three other methods, enhanced fuzzy classifier achieves higher detection accuracy since it maintained two partitions, low detection (L) and high detection (H) to obtain the detection accuracy level. The variance in the detection accuracy level is 8-10% high in the proposed Impulse noise detection and filtering using Enhanced Fuzzy Classifier.

### 3.3 Measure of Noise Level

The table 3.3.1 given below shows the level of noise present for different image sizes which is obtained using gray image of cameraman.

**Table 3.3.1 Measure of Noise level**

| Image Size (pixels) | Noise Level (%) |                |              |                 |
|---------------------|-----------------|----------------|--------------|-----------------|
|                     | Proposed INREFC | Entropy Filter | Range Filter | Standard Filter |
| 150                 | 75              | 78             | 80           | 85              |
| 200                 | 72              | 78             | 80           | 80              |
| 250                 | 60              | 70             | 71           | 75              |
| 300                 | 59              | 64             | 69           | 70              |

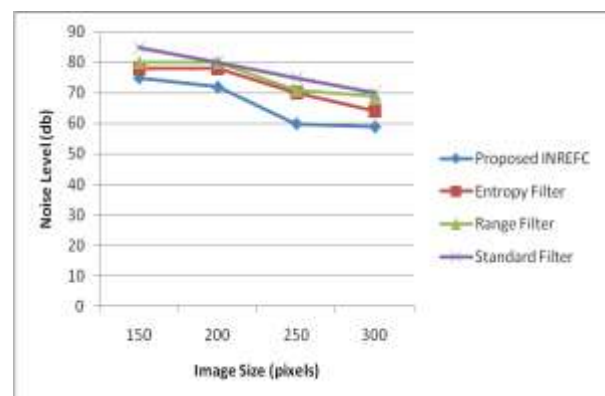


**Figure 3.3.1. Image Size Vs Noise Level**

Figure 3.3.1 describes the noise level of color and gray image applied to image of cameraman using Enhanced Fuzzy Classifier. The level of noise present in the color and gray images is measured in terms of decibels. The level of noise occurred in proposed INREFC is lesser when compared to other three methods due to the fact that the noise is removed using fuzzification and defuzzification process. The variance in the noise level is reduced 4-8% in the proposed Impulse noise detection and filtering using Enhanced Fuzzy Classifier when compared to entropy filter,

5-10% reduced when compared to range filter.

#### 4. CONCLUSION

An enhanced approach has been proposed for the removal of impulse noise using enhanced fuzzy classifier. The main advantages of this filter are the denoising capability and suitability for both gray and color images. A numerical measure, such as PSNR, detection accuracy, noise level have shown convincing results. Moreover, we have shown that the proposed method achieves a more comparable noise reduction performance than the other existing filters. Our future work will be on focusing reduction of speckle noise, stripping noise etc., in gray and color images.

#### 5. REFERENCES

- [1] Schulte, S V. De Witte, Nachtegael, M D. Van der Weken, and Kerre EE .2006. "Fuzzy random impulse noise reduction method", Fuzzy Sets and Systems vol 158 no 3 pp 270-283
- [2] Schulte, S, Morillas, V Gregori, Vand Kerre, EE .2007. "A new fuzzy color correlated impulse noise reduction Method" IEEE. Transactions on image Processing, Vol 16 No10, pp 2565-2575.
- [3] Morillas, S Gregori V and Sapena, A. 2006. "Fuzzy bilateral filtering for color images", Lecture Notes Comput. Sci., vol 4141, pp 138-145.
- [4] Schulte, S V. De Wite, Nachtegael M, Van den weken, D and Kerre EE. 2006. "Fuzzy Two step filter for impulse noise reduction from color images", IEEE. Transactions on image processing, vol 15.
- [5] Russo, F. 1999. "Fire operators for image processing," Fuzzy Sets Syst., vol. 103, no. 2, pp. 265-275.
- [6] Dimitri Van De Ville, Mike Nachtegael, Van der Weken, Etienne E. Kerre, Wilfried Philips and, Ignace Lemahieu. 2003. "Noise Reduction by Fuzzy Image Filtering.", IEEE Transactions on Fuzzy Systems, Vol. 11, No. 4 .
- [7] Nachtegael, M and Kerre, EE, Fuzzy mathematical morphology: state of the art, in: E.E. Kerre M. Nachtegael (Eds.) .2000. "Fuzzy Techniques in Image Processing, Studies in Fuzziness and Soft computing", vol. 52, Springer Verlag, Heidelberg., pp 3-57.
- [8] Lee, CS , Kuo VH & Yu PT. 1997. "Weighted fuzzy mean filters for image processing", Fuzzy sets and Systems, vol 89, pp. 157 - 180.
- [9] S. Schulte, B. Huysmans, A. Pizurica, EE, Kerre and W. Philips .2006. "A New Fuzzy Based wavelet shrinkage image denoising technique", Lecture Notes Computer science vol 41 no. 79 pp 12-23.

# THERMAL FATIGUE ANALYSIS OF INDUCTION MELTING FURNACE WALL FOR ALUMINA RAMMING MASS

N. C. Mehta  
Noble Engineering College  
Junagadh, India

Vasim G. Machhar  
Noble Engineering College  
Junagadh, India

Ravi K. Papat  
Noble Engineering College  
Junagadh, India

**Abstract:** Furnaces are most commonly used for melting of materials. Induction furnaces are more beneficial as no fuel is required. It is a problem to find life of Induction Melting Furnace wall under thermal fatigue. The induction melting furnace wall is made of alumina ramming mass which is one kind of refractory material. The failure occurs due to cyclic thermal stresses. Temperature distribution and thermal stress distribution fields of the induction melting furnace refractory wall were calculated by using ANSYS finite element analysis software based on the physical description of its failure under thermal fatigue conditions. The thermal fatigue life of the refractory wall is required to be found out by means of thermal stresses created inside the refractory wall of induction melting furnace from modified S – log N Curve.

**Keywords:** Thermal fatigue, induction furnace, finite element analysis, refractory, alumina ramming mass.

## 1. INTRODUCTION

### 1.1 FURNACE [1-3]

Furnace is a term used to identify a closed space here heat is applied to a body in order to raise its temperature. The source of heat may be fuel or electricity. Commonly, metals and alloys and sometimes non-metals are heated in furnaces. The purpose of heating defines the temperature of heating and heating rate.

Increase in temperature softens the metals. They become amenable to deformation. This softening occurs with or without a change in the metallic structure. Heating to lower temperatures (below the critical temperature) of the metal softens it by relieving the internal stresses. On the other hand, metals heated to temperatures above the critical temperatures leads to changes in crystal structures and re-crystallization like annealing. Further some metals and alloys are melted, ceramic products vitrified, coals coked, metals like zinc are vaporized and many other processes are performed in Furnaces.

### 1.2 DESCRIPTION OF PROBLEM

Induction furnaces are widely used in the iron industry for the casting of the different grades of cast iron products. Refractory wall of induction melting furnace is a key component which is used as insulation layer. It is made of ramming mass like alumina, alumina, magnesia etc. The refractory wall is directly influenced by the thermal cycling of the high temperature molten iron in the furnace. Thermal fatigue failure is easy to happen for it because of the larger phase transformation thermal stresses and it has a shorter life. This can cause serious production accidents. Therefore, the service life problem of the refractory wall has always been a focus of attention in the application of this to the industry.

The research on the distribution rule of temperature and thermal stress field and on the fatigue life assessment method for the refractory wall will not only lay foundation for the study on the thermal fatigue of this kind of parts under thermal shock condition of low cycle and high phase transition stresses but also offers effective control for thermal fatigue failure.

Here, ANSYS Software is used for finite element analysis of refractory wall. ANSYS calculates stress distribution across the refractory wall. The aim of this research is to identify points where critical stresses are generated so that we can minimize stresses in those regions and improve life of refractory wall.

## 2. LITERATURE REVIEW

Xia Zhou, Zhanfei Tanga and Guohui Qu<sup>4</sup> have done research work on thermal fatigue life of tundish cover. Continuous casting is widely used in the steel industry for the casting of different grades of steel products. Continuous casting tundish is a key intermediate device which is repeatedly used to store molten steel from melting furnace and then various steel section products are made by the continuous casting and rolling process, etc. The tundish cover is directly influenced by the thermal cycling of the high temperature molten steel in the tundish, so thermal fatigue failure is easy to happen for it because of the larger phase transformation thermal stress and it has a shorter life. This is not conducive to thermal insulation, cleanliness and pouring of liquid steel. What's more, this will cause serious production accidents.

Therefore, the service life problem of the tundish cover has always been a focus of attention in the application of this type of components to industry. The research on the distribution rule of temperature and thermal stress field and on the fatigue life assessment method for the tundish cover will not only lay foundation for the study on the thermal fatigue of this kind of parts under thermal shock condition of low cycle and high phase transition stress<sup>5</sup>, but also offer effective control for thermal fatigue failure.

To obtain high-quality continuous casting products, many researchers have studied steel flow, heat transfer and slag-steel interaction in tundishes under isothermal and non isothermal conditions by physical and mathematical modelling. Barron-Meza et al.<sup>6</sup> studied the effects and considerable changes of mixed convection flow in a tundish heated by a plasma torch using water modelling and mathematical simulation approaches. Mathematical simulations of the effects of a varying ladle stream temperature, heat losses and flow control devices on liquid steel flow patterns were reported by Morales et al.<sup>5</sup> and

Palafox-Ramos et al.<sup>5</sup> Solhed et al.<sup>5</sup> proposed a model of a tundish including the molten steel, slag, and refractory phases. The predictions of heat transfer and fluid-flow characteristics were validated by practical measurement data. In addition, fluid flow, heat and mass transfer of liquid steel in a trough type tundish were physically and mathematically simulated by Vargas-Zamora et al.<sup>11</sup> using water model. To the knowledge of the authors, neither the tundish nor the tundish cover has so far been included in any modeling efforts. It is obvious though, that thermal fatigue behavior of the tundish system especially the tundish cover will cause many metallurgical issues in the continuous casting process.

Traditional fatigue life prediction is often based on the statistical lifetime calculation of the large numbers of similar products or on lots of physics experiments, while these two methods are both time-consuming and high cost. In recent years, many scholars have also proposed other methods for evaluating fatigue damage such as the crack propagation methods based on the fracture theory<sup>12–16</sup> and the finite element methods based on the damage mechanics<sup>5</sup> However, there still exist some problems when the above-mentioned methods applied to fatigue life analysis: firstly a simplified two-dimensional (2D) model is often used in most methods; secondly no kinds of methods can be totally suitable for the life estimation of structures particularly practical structures subjected to accumulated fatigue damage. In practical engineering, the simplified plane model is often unreasonable because of prominent fatigue problems and geometrical configuration of complex structures. So research on an efficient and accurate fatigue life prediction method has great significance to identify the mechanism of materials or structural failure and improve product life.

### 3. PREPROCESSING OF FEA USING ANSYS

The accurate simulation of Induction melting furnace refractory wall is done for finding out temperature distribution and thermal stress distribution by using proper solving conditions. These solving conditions include initial and boundary conditions, material properties and assumptions etc. Finite Element Analysis using ANSYS was performed to calculate temperature field and stress field caused by application of heat flux caused by heat generation inside the induction melting furnace.

#### 3.1 ANALYSIS MODEL

Based on drawing and dimensions available from Jyoti CNC Limited, a model is developed using Pro E software and radius is given to minimize effects of heat concentration on edges. We had converted this model in iges format which is universal format for all modeling software then it is imported into ANSYS.

#### 3.2 MESH SIZE SELECTION

We have done coupled field dynamic analysis using different mesh size and found that with the increase in mesh density stress is decreasing up to an optimum value but then if we go for more mesh density then stress will increase. We have done three kinds of meshing course, normal and fine meshing. In course meshing, we had selected 2689 nodes and 1197 elements and we had got maximum stress 223 MPa. Then we had selected normal mesh density 10,018 elements and 17,425 nodes and we had got maximum stresses 176 MPa. In very fine meshing, we had selected 79,773 elements and 1,22,459 nodes and we had got 189 MPa maximum stresses. So we understand that we are going away from the answer so that

we had selected normal mesh density. If we go for very fine meshing or very course meshing we will go away from the accuracy. So that we had selected mesh density which will give be more nearer to the actual value. Thus we had found out mesh density.

### 3.3 INITIAL AND BOUNDARY CONDITIONS, MATERIAL PROPERTIES AND BASIC ASSUMPTIONS

To solve this heat transfer problem of induction melting furnace wall, the following initial and boundary conditions, material properties and basic assumptions are made:

- Refractory Materials for induction furnace wall meets the basic assumptions in the science of mechanics.
- Environmental Temperature is homogeneous at 25° C.
- Ignore the influence of heat convection.
- Ignore the effect of gravity field.
- The surface of induction melting furnace wall is clean.
- The initial temperature of the induction melting furnace is set 25° C and it is agreement with the ambient temperature during solving the problem.
- Heat flux is considered constant for this analysis.
- Scarp material input inside furnace is considered uniform for our analysis.

#### Calculation of Heat Flux:

- Heat Flux = Heat Generated / Area
- Heat Flux =  $Q_g / (2\pi r^2 l)$
- Heat Flux =  $150 \text{ kw} / (2 \times 3.14 \times 0.3715 \times 1.21) \text{ m}^2$
- Heat Flux = 150 / 2.82 kw/ m<sup>2</sup>
- Heat Flux = 53,000 watt/ m<sup>2</sup>

### 4.0 RESULTS AND DISCUSSION

It gives temperature distribution and stress distribution for four different materials alumina ramming mass. It indicates that temperature at inner side of the furnace wall is higher than at outside of the furnace wall.

We had entered material properties of alumina ramming mass. We had found out temperature distribution after 1 hour, 2 hour and 3 hour. We had plotted a graph of change in temperature with respect to time at inner surface and outer surface of the furnace wall. We had found out stress distribution after 20 minutes, 40 minutes and 60 minutes.

We had plotted a graph of stress variation with respect to time at inner surface and outer surface of furnace wall. The red colour in the stress distribution diagrams indicate maximum stresses created and from that region minor crack propagation will be started for fatigue failure.

Table 1. Table captions should be placed above the table

| Material Properties Of Alumina Ramming Mass |                     |      | Unit              |
|---|---------------------|------|-------------------|
| 1   | Elasticity Constant | 222  | GPa               |
| 2   | Poisson's Ratio     | 0.22 | -                 |
| 3   | Density             | 3400 | KG/m <sup>3</sup> |

|   |                                |     |                              |
|---|--------------------------------|-----|------------------------------|
| 4 | Thermal Expansion Co-efficient | 7.2 | $\mu\text{M}/^\circ\text{C}$ |
| 5 | Thermal Conductivity           | 11  | watt/m k                     |
| 6 | Specific Heat                  | 950 | J/kg K                       |

#### 4.1 RESULTS OF TEMPERATURE DISTRIBUTION

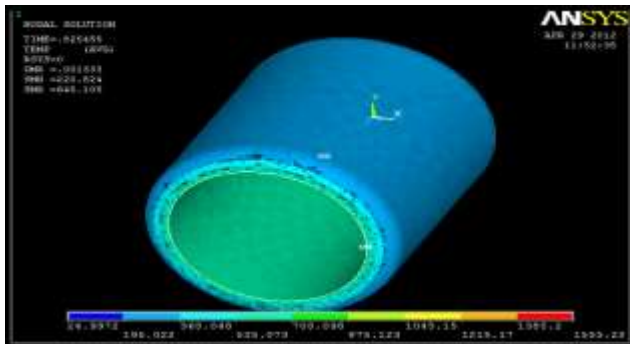


Figure 4.1 Temp distributions in furnace wall after 1 hour for alumina ramming mass

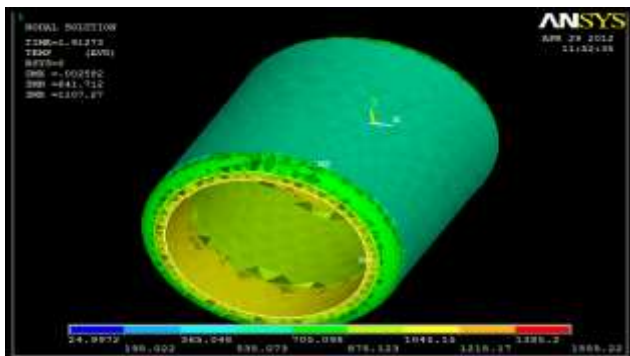


Figure 4.2 Temp distributions in furnace wall after 2 hour for alumina ramming mass

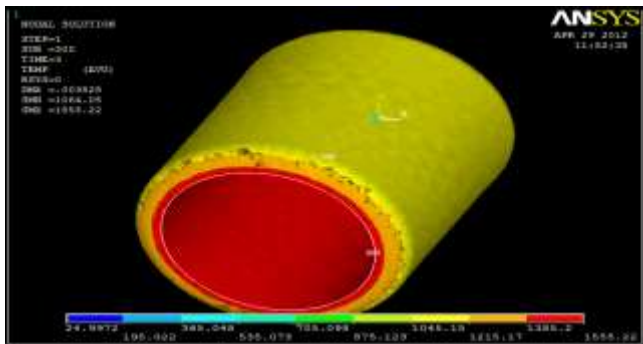


Figure 4.3 Temp distributions in furnace wall after 3 hour for alumina ramming mass

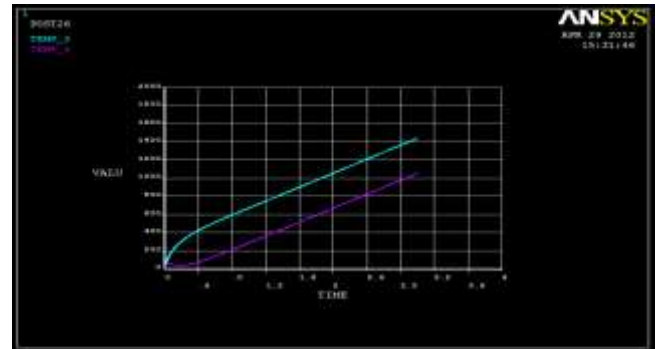


Figure 4.4 Temperature inside and outside furnace wall for alumina ramming mass

#### 4.2 RESULTS OF THERMAL STRESS DISTRIBUTION

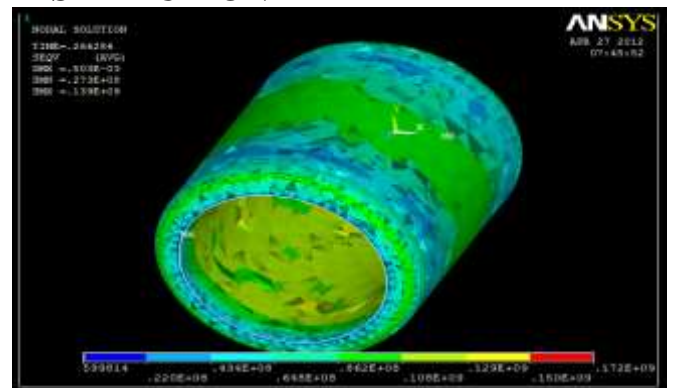


Figure 4.5 Stress distributions in furnace wall after 20 minutes for alumina ramming mass

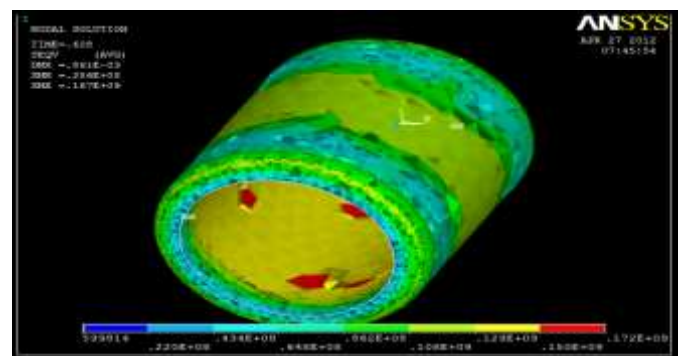


Figure 4.6 Stress distributions in furnace wall after 40 minutes for alumina ramming mass

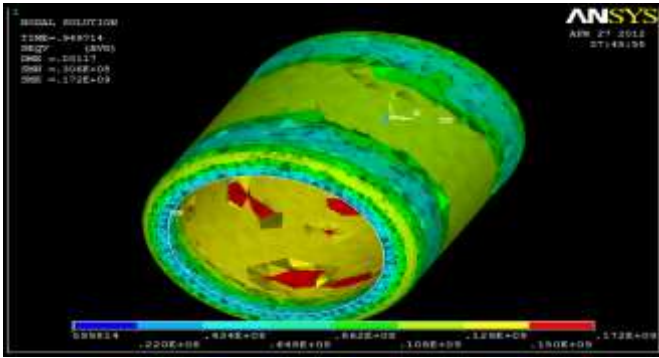


Figure 4.7 Stress distributions in furnace wall after 60 minutes for alumina ramming mass

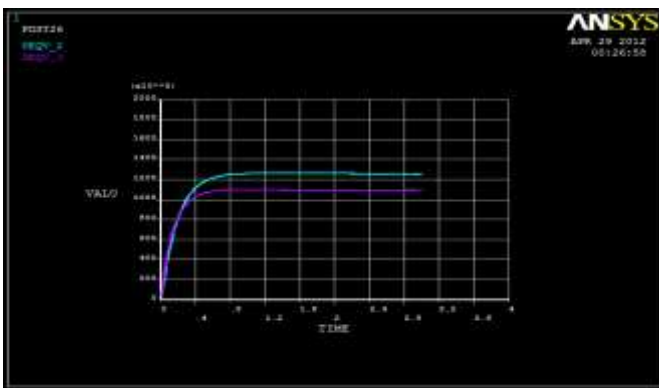


Figure 4.8 Stress outside and inside furnace wall for alumina ramming mass

## 5.0 PREDICTION OF THERMAL FATIGUE LIFE

### 5.1 FATIGUE LIFE METHODS [6]

The three major fatigue life methods used in design and analysis are the stress-life method, the strain-life method, and the linear-elastic fracture mechanics method. These methods attempt to predict the life in number of cycles to failure,  $N$ , for a specific level of loading. Life of  $1 \leq N \leq 10^3$  cycles is generally classified as low-cycle fatigue, whereas high-cycle fatigue is considered to be  $N > 10^3$  cycles. The stress-life method, based on stress levels only, is the least accurate approach, especially for low-cycle applications. However, it is the most traditional method, since it is the easiest to implement for a wide range of design applications, has ample supporting data, and represents high cycle applications adequately.

The strain-life method involves more detailed analysis of the plastic deformation at localized regions where the stresses and strains are considered for life estimates. This method is especially good for low-cycle fatigue applications. In applying this method, several idealizations must be compounded, and so some uncertainties will exist in the results. For this reason, it will be discussed only because of its value in adding to the understanding of the nature of fatigue.

The fracture mechanics method assumes a crack is already present and detected. It is then employed to predict crack growth with respect to stress intensity. It is most practical when applied to large structures in conjunction with computer codes and a periodic inspection program.

### 5.2 THE STRESS-LIFE METHOD

To determine life of any component by Stress-Life Method, we need to find out ultimate strength and endurance limit of the component for the required material.

We know the values of ultimate stress for these all materials. Alumina ramming mass is having ultimate strength of 272 MPa. We can find out  $Se'$  from the equation given below or we can say dividing value of ultimate strength.

We know value of ultimate stress of the material.

| Material             | $S_{ut}$ (MPa) |
|----------------------|----------------|
| alumina ramming mass | 271            |

We know the relation between  $S_{ut}$  and  $Se'$  so that we can find out  $Se'$ .

$$Se' = 0.5 * S_{ut}$$

| Material             | $Se'$ (MPa) |
|----------------------|-------------|
| alumina ramming mass | 135.5       |

Endurance Limit Modifying Factors:

We have seen that the rotating-beam specimen used in the laboratory to determine endurance limits is prepared very carefully and tested under closely controlled conditions.

It is unrealistic to expect the endurance limit of a mechanical or structural member to match the values obtained in the laboratory.

Some differences include

- Material: composition, basis of failure, variability
- Manufacturing: method, heat treatment, fretting corrosion, surface condition, stress concentration
- Environment: corrosion, temperature, stress state, relaxation times
- Design: size, shape, life, stress state, stress concentration, speed, fretting, galling.

Marin identified factors that quantified the effects of surface condition, size, loading, temperature, and miscellaneous items. The question of whether to adjust the endurance limit by subtractive corrections or multiplicative corrections was resolved by an extensive statistical analysis of a 4340 (electric furnace, aircraft quality) steel, in which a correlation coefficient of 0.85 was found for the multiplicative form and 0.40 for the additive form.

A Marin equation is therefore written as

$$Se = k_a \times k_b \times k_c \times k_d \times k_e \times k_f \times Se'$$

Where,

$k_a$  = surface condition modification factor

$k_b$  = size modification factor

$k_c$  = load modification factor

$k_d$  = temperature modification factor

$k_e$  = reliability factor

$k_f$  = miscellaneous-effects modification factor

Se' = specimen endurance limit

Se = endurance limit at the critical location of a machine part in the geometry and condition of use

We can find out different as per the guideline given in the Machine Engineering Design by Shigley.[19]

|                                    |      |
|------------------------------------|------|
| Surface Finish Factor $k_a$        | 0.86 |
| Size Factor $k_b$                  | 1    |
| Loading Factor $k_c$               | 1    |
| Temperature Factor $k_d$           | 0.25 |
| Reliability Factor $k_e$           | 0.9  |
| Miscellaneous Effects Factor $k_f$ | 1    |

Now, we can find out endurance limit for all different materials.

$$Se = k_a \times k_b \times k_c \times k_d \times k_e \times k_f \times Se'$$

| Material             | Se (MPa) |
|----------------------|----------|
| alumina ramming mass | 26.21    |

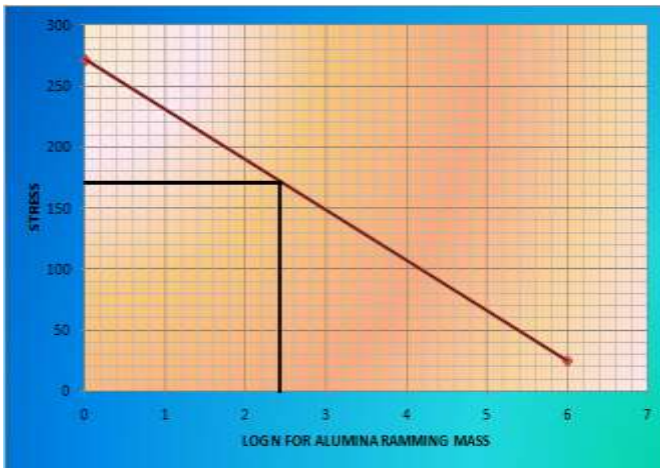


Figure 5.1 Modified S – Log N Curve for Alumina Ramming Mass

## 6.0 CONCLUSION

Induction Melting Furnaces are highly used now- a-days for melting of different kinds of materials. The problem comes from the Refractory material of losing its thermal properties

within 200-400 hours of lifetime. It will disturb production schedule as it requires time to replace the Induction melting furnace wall. Coupled Field Analysis is done for Induction Melting Furnace Refractory Wall and validation is done with respect to Experimental Results. Coupled Field Analysis is done with respect to Alumina Ramming Mass. Then S – log N Curves are plotted for Life Span Prediction.

We had found life span of different materials like alumina ramming mass 200 cycles. From the results of experimental study and finite element simulation of thermal fatigue failure of induction melting furnace wall, it can be seen that finite element simulation exactly predicts the failure of the induction furnace refractory wall and the definite solution conditions in the finite element numerical calculation are accurate.

The fatigue life of the induction melting furnace refractory wall under thermal fatigue working conditions was predicted using Stress-Life Method by plotting S – log N curves for different materials on the basis of finite element calculations and maximum stress in the induction melting furnace refractory wall. We can use it as a linear to increase lifespan or we can use premixed ramming mass for economical and better working lifespan of induction melting furnace wall.

The accuracy of the fatigue life prediction for the induction melting furnace refractory wall depends upon stress spectrum calculated at the critical point by finite element method and on S-log N fatigue curves prepared from the material properties of different materials.

## 7.0 REFERENCES

- [1] John Campbell, Castings (2nd Edition)
- [2] Peter Mullinger and Barrie Jenkins, Industrial and Process Furnaces (1st Edition) Elsevier Publication
- [3] A V K Suryanarayana, Fuels Furnaces Refractory and Pyrometry B S Publications
- [4] Xia Zhoua,, Zhanfei Tanga, Guohui Qu “Thermal stress and thermal fatigue analysis of the continuous casting tundish cover”, November 2009
- [5] Thermal Fatigue Analysis of Induction Melting Furnace Wall for Silica Ramming Mass, Prof. N. C. Mehta, A.D. Raiyani, V.R. Gondaliya, IJETAE, Volume 3, Issue 2, February 2013
- [6] Machine Engineering Design by Joseph E. Shigley and Charles R. Mischke, TATA McGRAW HILL Publication, sixth edition